Molecular Mechanics Study of Oligomeric Models for Poly(ferrocenylsilanes) Using the Extensible Systematic Forcefield (ESFF)

Stephen Barlow,[†] Andrew L. Rohl,[†,‡] Shengua Shi,[§,⊥] Clive M. Freeman,[⊥] and Dermot O'Hare*[,†]

Contribution from the Inorganic Chemistry Laboratory, South Parks Road, Oxford, OX1 3QR, UK, and Molecular Simulations, Inc., 9685 Scranton Road, San Diego, California 92121

Received November 1, 1995. Revised Manuscript Received May 7, 1996[⊗]

Abstract: Molecular mechanics have been employed to study the conformations of the oligomeric metallocene species $Fc[Fe(C_5H_4)_2XMe_2]_nH$ (Fc = $Fe(C_5H_5)(C_5H_4)$; X = Si, n = 1 (**1**); X = C, n = 1 (**2**); X = Si, n = 2 (**3**); X = C, n = 2 (**4**); X = Si, n = 4 (**5**)) and their cations. The calculations utilize the new generalized ESFF forcefield; they show that the neutral molecules are conformationally flexible with the lowest energy configurations having close contacts between the positively charged iron atoms of the ferrocene units and the negatively charged cyclopentadienyl rings of their neighbors. The carbon-bridged species have harder potential surfaces than their silicon analogues, but replacement of the methyl groups of the bridge with longer alkyl chains was found to have very little effect on the relative orientation of the ferrocene units. The conformations of the molecules **3**, **4**, and **5** in their experimental crystal structures were found to be significantly different from the calculated low energy isolated conformers. However, the solid state conformations allow *inter*molecular iron−cyclopentadienyl interactions analogous to the *intra*molecular interactions found for the isolated species. In contrast, the conformation of $(\mathbf{3})^{3+}$ in the crystal structure is very similar to the calculated low energy isolated conformer, since the conformations are primarily determined by Fe−Fe repulsion. Implications of this work for the structures of high-molecular weight poly(ferrocenylsilanes) are discussed.

Introduction

Since the first thermal ring-opening polymerization reactions (Figure 1) of [1]silaferrocenophanes were reported in 1992,[1] high molecular mass poly(ferrocenylsilanes) have attracted considerable interest as rare examples of polymers incorporating transition metals in the backbone.[2,3] The properties of the polymers may be varied by altering the substituents on the silicon bridge[4−6] and by varying the degree of methylation of the cyclopentadienyl rings.[7] The ring-opening polymerization reaction has also been extended to ferrocenophanes with germanium,[8,9] phosphorus,[10] and sulfur bridges[11] and to hydrocarbon-bridged ferrocenophanes[12] and ruthenocenophanes.[13] The reaction has also been accomplished at low temperatures with anionic initiators,[14] with γ-irradiation,[15] and with transition metal catalysts;[16,17] the former methodology has permitted the synthesis of copolymers incorporating blocks of poly(ferrocenylsilane).[18] Poly(ferrocenylsilanes) are of interest due to their potentially interesting optical, electronic and magnetic behavior. Doped materials have so far shown low conductivities, but modification of the bridging groups is anticipated to offer possible routes to electronically delocalized materials.[2] The reaction of low molecular weight poly(ferrocenylsilanes) and tetracyanoethylene has been reported to yield a ferromagnetic material.[19] Pyrolysis of certain poly(ferrocenylsilanes) has yielded novel iron−silicon−carbon ceramics.[20,21]

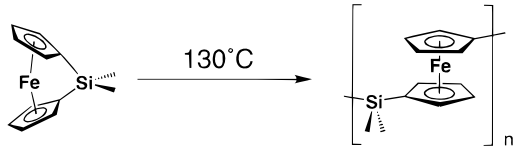

Figure 1. Ring-opening polymerization of a strained ferrocenophane.

* To whom correspondence should be addressed. D. O'Hare is the Sir Edward Frankland Fellow of the Royal Society of Chemistry.
[†] Inorganic Chemistry Laboratory.
[‡] Present address: Department of Applied Chemistry, Curtin University of Technology, P.O. Box U 1987, Perth, 6001, Western Australia.
[§] Present address: ALANEX Corporation, 3550 General Atomics Court, San Diego, CA 92121.
[⊥] Molecular Simulations, Inc.
[⊗] Abstract published in *Advance ACS Abstracts,* July 1, 1996.

(1) Foucher, D. A.; Tang, B.-Z.; Manners, I. *J. Am. Chem. Soc.* **1992**, *114*, 6246−6248.
(2) Manners, I. *Adv. Mater.* **1994**, *6*, 68−71 and references therein.
(3) Manners, I. *Chem. Br.* **1996**, *32*, 46−49 and references therein.
(4) Foucher, D. A.; Ziembinski, R.; Tang, B.-Z.; Macdonald, P. M.; Massey, J.; Jaeger, C. R.; Vansco, G. J.; Manners, I. *Macromolecules* **1993**, *26*, 2878−2884.
(5) Foucher, D.; Ziembinski, R.; Petersen, R.; Pudelski, J.; Edwards, M.; Ni, Y. Z.; Massey, J.; Jaeger, C. R.; Vansco, G. J.; Manners, I. *Macromolecules* **1994**, *27*, 3992−3999.
(6) Nguyen, M. T.; Diaz, A. F.; Dement'ev, V. V.; Pannell, K. H. *Chem. Mater.* **1993**, *5*, 1389−1394.
(7) Pudelski, J. K.; Foucher, D. A.; Macdonald, P. M.; Honeyman, C. H.; Manners, I.; Barlow, S.; O'Hare, D. *Macromolecules* **1996**, *29*, 1894−1903.
(8) Foucher, D. A.; Manners, I. *Makromol. Chem., Rapid Commun.* **1993**, *14*, 63−66.
(9) Foucher, D. A.; Edwards, M.; Burrow, R. A.; Lough, A. J.; Manners, I. *Organometallics* **1994**, *13*, 4959−4966.
(10) Honeyman, C. H.; Foucher, D. A.; Dahmen, F. Y.; Rulkens, R.; Lough, A. J.; Manners, I. *Organometallics* **1995**, *14*, 5503−5512.
(11) Pudelski, J. K.; Gates, D. P.; Rulkens, R.; Lough, A. J.; Manners, I. *Angew. Chem., Int. Ed. Engl.* **1995**, *34*, 1506−1508.
(12) Nelson, J. M.; Rengel, H.; Manners, I. *J. Am. Chem. Soc.* **1993**, *115*, 7035−7036.
(13) Nelson, J. M.; Lough, A. J.; Manners, I. *Angew. Chem., Int. Ed. Engl.* **1994**, *33*, 989−991.
(14) Rulkens, R.; Lough, A. J.; Manners, I. *J. Am. Chem. Soc.* **1994**, *116*, 797−798.
(15) Rasburn, J.; Petersen, R.; Jahr, T.; Rulkens, R.; Manners, I.; Vansco, G. J. *Chem. Mater.* **1995**, *7*, 871−877.
(16) Ni, Y.; Rulkens, R.; Pudelski, J. K.; Manners, I. *Makromol. Chem., Rapid Commun.* **1995**, *16*, 637.
(17) Reddy, N. P.; Yamashita, H.; Tanaka, M. *J. Chem. Soc., Chem. Commun.* **1995**, 2263−2264.
(18) Rulkens, R.; Ni, Y. Z.; Manners, I. *J. Am. Chem. Soc.* **1994**, *116*, 12121−12122.
(19) Hmyene, M.; Yasser, A.; Escorne, M.; Percheron-Guegan, A.; Garnier, F. *Adv. Mater.* **1994**, *6*, 564−568.

S0002-7863(95)03680-8 CCC: $12.00

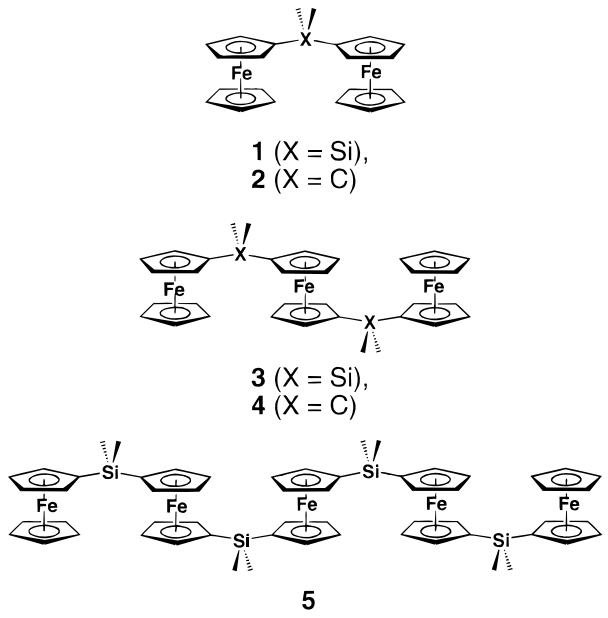

Figure 2. The oligomeric metallocenes in this study.

An understanding of the preferred conformations of poly(ferrocenylsilanes) would greatly aid the rationalization of the properties of these materials including their glass transition temperatures, which have been found to be dependent upon the nature of the substituents on the silicon bridges,[4,5] and their electrochemical behavior. It has been found that poly(ferrocenylsilanes) show two oxidation waves reflecting interactions between the ferrocene centers; the separation of these waves, ΔE, varies with the nature of the substituents on the silicon bridge. Two possible explanations for this variation have been proposed: different inductive effects on the electronic structure of the bridge of different substituents or differing iron−iron separations owing to different conformations of the polymers.[22] Knowledge of the preferred conformations of both neutral and oxidized polymers may shed light on this problem.

Recently short chain oligomers have been studied as models for the conformational and electrochemical behavior of high polymers (Figure 2). Rulkens *et al.* used the reaction of lithioferrocene and $Fe(C_5H_4)_2SiMe_2$ to synthesize a range of oligomers comprising between two and eight ferrocene units bridged by $SiMe_2$ groups;[14] they determined the crystal structures of the trimeric (**3**)[23] and pentameric (**5**)[14] species. Pannell *et al.* have also synthesized **3** by two alternative routes: the reaction of lithioferrocene and 1,1′-bis(chlorodimethylsilyl)ferrocene and the reaction of dilithioferrocene and (chlorodimethylsilyl)ferrocene and determined its crystal structure.[24] They also performed molecular mechanics calculations to illustrate the range of conformers possible in such systems. As part of an investigation of the magnetic properties of oligometallocenium salts, we recently reported the syntheses and crystal structures of the CMe_2 bridged analogue of **3**, denoted **4**, and its trication.[25] The structure of the neutral species exhibited a markedly different conformation of the trimetallocene unit from **3** and the three highly symmetric minimum energy configurations calculated by Pannell *et al.* Thus we performed our own calculations on the conformations of a series of oligometallocenes and report the results here.

Calculation Section

Potential Parameters. Molecular mechanics[26,27] is a powerful and widely used tool for studying the conformations and solid state structures of organic,[28] biological,[29] and polymer systems.[30] The success of the technique is founded upon the derivation of transferable potential parameters which accurately describe both the intra- and intermolecular forces of a given system. Such a parameter set, or *forcefield*, may be determined by parameter optimization, or fitting, with the objective of reproducing *ab initio* quantum chemical properties and/or experimental observation for appropriate representative molecules. For example, the MM forcefields were originally parameterized for organic compounds,[31] whilst the AMBER forcefield was designed for applications in protein and nucleic acid[32] modeling. To transfer potentials to systems outside the original scope of a forcefield demands further parameter refinement and validation which can be a time consuming process. There is, however, considerable demand for forcefields able to treat metalloproteins, inorganic systems, and organometallic complexes of transition metals. Since there are many transition metal atoms, with diverse coordination numbers and geometries, the development of forcefields for such systems poses a considerable challenge. However, some traditional organic forcefields have been extended to systems such as simple sandwich metallocenes MCp_2,[33] metallocene dichlorides (MCp_2Cl_2),[34] [1.1]ferrocenophanes,[35] multiply bridged ferrocenophanes,[36] square planar Pt complexes,[37] and Cu(II) complexes.[38] The ESFF (Extensible Systematic ForceField)[39] employed in the present study uses a rule based algorithm to determine a potential parameter set for a given system. This approach relies on a modest set of atomic parameters which are then used to generate a complete system specific forcefield through a series of empirical rules. The resulting potential parameters are used to calculate molecular energies and stabilites as a sum of contributing energy terms according to the following expressions:

(20) Tang, B.-Z.; Petersen, R.; Foucher, D. A.; Lough, A.; Coombs, N.; Sodhi, R.; Manners, I. *J. Chem. Soc., Chem. Commun.* **1993**, 523−525.
(21) Petersen, R.; Foucher, D. A.; Lough, A. J.; Manners, I. *Phosphorus, Sulfur and Silicon and the Related Elements* **1994**, *93*, 359−360.
(22) Foucher, D. A.; Honeyman, C. H.; Nelson, J. M.; Tang, B. Z.; Manners, I. *Angew. Chem., Int. Ed. Engl.* **1993**, *32*, 1709−1711.
(23) Lough, A. J.; Manners, I.; Rulkens, R. *Acta Crystallogr.* **1994**, *C50*, 1667−1669.
(24) Pannell, K. H.; Dementiev, V. V.; Li, H.; Cervantes-Lee, F.; Nguyen, M. T.; Diaz, A. F. *Organometallics* **1994**, *13*, 3644−3650.
(25) Barlow, S.; Murphy, V. J.; Evans, J. S. O.; O'Hare, D. *Organometallics* **1995**, *14*, 3461−3474.
(26) Grant, G. H.; Richards, W. G. *Computational Chemistry, Chapter 3*; OUP: Oxford, 1995.
(27) Bukert, U.; Allinger, N. L. *Molecular Mechanics, ACS Monograph 177*; American Chemical Society: Washington, 1982.
(28) Desiraju, G. R. *Crystal Engineering: The Design of Organic Solids*; Elsevier: Amsterdam, 1989.
(29) Li, H.; Poulos, T. L. *Acta Crystallogr.* **1995**, *D51*, 21−32.
(30) Ferro, D. R.; Ragazzi, M.; Bruckner, S.; Meille, S. V. *Macromolecular Symposia* **1995**, *89*, 529−542.
(31) Allinger, N. L.; Yuh, Y. H.; Lii, J. H. *J. Am. Chem. Soc.* **1989**, *111*, 8551−8566.
(32) Weiner, S. J.; Kollman, P. A.; Case, D. A.; Singh, U. C.; Ghio, C.; Alagona, G.; Profeta, S.; Weiner, P. *J. Am. Chem. Soc.* **1984**, *106*, 765−784.
(33) Doman, T. N.; Landis, C. R.; Bosnich, B. *J. Am. Chem. Soc.* **1992**, *114*, 7264−7272.
(34) Doman, T. N.; Hollis, T. K.; Bosnich, B. *J. Am. Chem. Soc.* **1995**, *117*, 1352−1368.
(35) Rudzinski, J. M.; Osawa, E. *J. Phys. Org. Chem.* **1993**, *6*, 107−112.
(36) Rudzinski, J. M.; Osawa, W. *J. Phys. Org. Chem.* **1992**, *5*, 382−394.
(37) Castonguay, L. A.; Rappé, A. K.; Casewit, C. J. *J. Am. Chem. Soc.* **1991**, *113*, 7177−7183.
(38) Burton, V. J.; Deeth, R. J. *J. Chem. Soc., Chem. Commun.* **1995**, 573−574.
(39) Shi, S.; Yan, L.; Shaulsky, J.; Thacher, T. A New Forcefield, ESFF, for Molecular Modalling of Organic, Inorganic and Organometallic Systems. Manuscript in preparation.

Bond Energy. The bond stretching is described by a Morse function

$$E = \sum_b D_b\{1 - \exp(1 + \alpha(r_b - r_b^o))\}^2 \qquad (1)$$

where D_b is the bond dissociation energy, r_b^o is the bond reference value, and α characterizes the bond anharmonicity. Bond types are specified according to bond orders (dative, single, partial double, double, or triple) and symmetry positions (axial or equatorial).

Angle Energy. To facilitate the description of unconventional structures resulting from d−p π bonding between unsaturated ligands (L) and transition metals (M), the concept of pseudoangles is introduced. Pseudoangles are defined as angles having at least one pseudobond. Used only for angle energy calculations, a pseudobond connects a pseudoatom with the central metal atom. The pseudoatom represents a group of connected real atoms which all bond to one metal atom with their delocalized π orbitals. For example, a pseudoatom would be placed at the centroid of an η^5-cyclopentadienyl ring. Both pseudoangles and bond angles are classified in accordance with the symmetry positions of the two constitutuent bonds: (1) the linear angle type includes angles with central atoms having sp hybridization as well as angles with two axial bonds ($L_{ax}-M-L_{ax}$); (2) the perpendicular class is restricted to angles with one axial bond and one equatorial bond ($L_{ax}-M-L_{eq}$); (3) the equatorial type describes angles between two equatorial bonds ($L_{eq}-M-L_{eq}$); (4) angles that do not belong to any of the above three types are included in the class of normal angles. The nonpseudonormal angles are further specified according to the ring information of whether the angle is unconstrained or is an endo- or exo- angle of a three-, four-, or five-membered ring. The following cosine forms have been chosen for the expressions of angle energy.

$$E_a = \begin{cases} \sum_a \dfrac{K_a}{\sin^2 \theta_a^o}(\cos\theta_a - \cos\theta_a^o)^2 & \text{normal (2.1)} \\ \sum_a 2K_a(\cos\theta_a + 1) & \text{linear (2.2)} \\ \sum_a K_a \cos^2\theta_a & \text{perpendicular (2.3)} \\ \sum_a \dfrac{2K_a}{n^2}[1 - \cos(n\theta_a)] + 2K_a \exp[-\beta(r_{13} - \rho_a)] & \text{equatorial (2.4)} \end{cases}$$

In eq 2.1 θ_a^o is the reference angle value determined from the angle atomic parameters of the terminal atoms as well as the central atom. The atomic parameters for the terminal atoms depend on their atom types and bond orders, while the atomic parameter for the central atom is determined according to its atom type and ring information. The K_a in eq 2 is the force constant which is determined by the atom types of the terminal and central atoms. The second term on the right side of eq 2.4 represents a repulsion barrier preventing two bonds from overlapping since $\theta_a = 0$ is a minimum for the first term. In the first term, n is characteristic of a given symmetry, e.g., $n = 4$ for a complex with D_{4h} symmetry.

Torsion Energy. The torsional energy is given by the following expression

$$E_t = \sum_t D_t\left(\frac{\sin^2\theta_1 \sin^2\theta_2}{\sin^2\theta_1^0 \sin^2\theta_2^0} + sign\frac{\sin^n\theta_1 \sin^n\theta_2}{\sin^n\theta_1^0 \sin^n\theta_2^0}\cos[n\tau]\right) \qquad (3)$$

where τ is a torsion angle and θ_1 and θ_2 are the associated bond angles. Equation 3 has two advantages over traditional molecular mechanics torsional forms. First, the torsion energy approaches zero smoothly and is free of the derivative singularity[40] when θ_1 or θ_2 approaches π. Secondly, the τ-dependent numerator in the second term, $\sin^n\theta_1 \sin^n\theta_2 \cos[n\tau]$, can be expressed in terms of $\cos^2\theta_1$, $\cos^2\theta_2$ and a function $F(\theta,\tau) = \sin\theta_1 \sin\theta_2 \cos\tau$ which, in turn, can be written as a product of unit vectors along the bonds 1−2, 2−3, and 3−4:

$$F(\theta,\tau) = (\hat{r}_{12} \times \hat{r}_{23})\cdot(\hat{r}_{23} \times \hat{r}_{34}) = (\hat{r}_{12}\cdot\hat{r}_{23})\cdot(\hat{r}_{23}\cdot\hat{r}_{34}) - (\hat{r}_{12}\cdot\hat{r}_{34}) \qquad (4)$$

Therefore, the torsion energy can be expressed in terms of dot products of the unit vectors, $\hat{r}_{12}$, $\hat{r}_{23}$ and $\hat{r}_{34}$ which considerably simplifies the calculation of the energy and its Cartesian derivatives.

Out-of-Plane Energy. The expression used for the OOP energy is

$$E_o = \sum_o D_o \phi^2 \qquad (5)$$

where the force constant D_o depends only on the atom type of the central atom, and ϕ is the Wilson OOP angle.[41]

VDW Interaction Energy. The energy expression for the VDW interaction takes the Lennard-Jones 6−9 type of form

$$E_{vdw} = \sum_{i=1}^{N}\sum_{j\neq 1}^{N}\left[\frac{A_iB_j + A_jB_i}{r_{ij}^9} - 3\frac{B_iB_j}{r_{ij}^6}\right] \qquad (6.1)$$

with

$$A_i = \sqrt{\epsilon_i} r_i^{o6} \qquad (6.2)$$

and

$$B_i = \sqrt{\epsilon_i} r_i^{o3} \qquad (6.3)$$

where r_i^o and ϵ_i are the VDW radius and well depth for atom i respectively and N is the number of atoms in the system of interest. Note that within molecules, these VDW interactions are only calculated between 1−4 neighbors and higher.

Electrostatic Energy. The electrostatic energy is calculated according to Coulomb's law

$$E_{es} = \sum_{i=1}^{N}\sum_{j\neq 1}^{N} q_i q_j / r_{ij} \qquad (7)$$

where q_i and q_j are the atomic partial charges on atom i and j and r_{ij} is the distance between atom i and atom j. Similarly to the case for the VDW interactions, the Coulombic interactions within molecules are only calculated between 1−4 neighbors and higher. The partial charges q_i are derived from two fundamental atomic parameters, the electronegativity χ_i and hardness η_i, which are defined as the first and second derivative of the atomic energy with respect to the atomic charge, respectively. Partial charges are, however, topology dependent and are determined at the outset of a molecular mechanics calculation using an electronegativity equalization[42] scheme. This procedure takes into account inductive, resonance and longer range effects in assigning partial charges.

(40) Swope, W. C.; Ferguson, D. M. *J. Comput. Chem.* **1992**, *13*, 585−594.

(41) Wilson, E. B.; Decius, J. C.; Cross, P. C. *Molecular Vibrations*; Dover: New York, 1980.

(42) Gasteiger, J.; Marsili, M. *Tetrahedron* **1980**, *36*, 3219.

Table 1. Partial Charges for Atoms in $Fc[Fe(C_5H_4)_2XMe_2]_nH$ (Fc = $Fe(C_5H_5)(C_5H_4)$; X = Si, $n = 1$ (**1**); X = C, $n = 1$ (**2**); X = Si, $n = 2$ (**3**); X = C, $n = 2$ (**4**); X = Si, $n = 4$ (**5**))

	X = C		X = Si	
atom[a]	neutral	cation	neutral	cation
Fe	1.250	1.568	1.250	1.568
X	−0.075	−0.051	−0.182	−0.126
C_5H_5(C)	−0.180	−0.140	−0.180	−0.140
C_5H_4X(1-C)	−0.206	−0.160	−0.083	−0.049
C_5H_4X(2,5-C)	−0.146	−0.106	−0.189	−0.148
C_5H_4X(3,4-C)	−0.180	−0.140	−0.180	−0.140
Me(C)	−0.081	−0.070	−0.023	−0.017
Cp(H)	0.055	0.083	0.055	0.083
Me(H)	0.044	0.044	0.030	0.030

[a] Atoms in parentheses are the particular atoms in the fragment which the values relate to.

Parameterization. The atomic parameters used to generate the potential parameters were determined by a procedure which involved density functional theory (DFT) calculations, fitting experimental data, and fitting crystal structures and their properties. The basic DFT calculated parameters are electronegativity χ, hardness η, and ionization potential IP. These parameters were determined for each atom type based on the hybridization of atoms and the distribution of valence electrons in the hybridized orbitals. Having calculated these basic atomic parameters, the nonbonded atomic parameters were generated by fitting the crystal lattice constants and their available properties (e.g., sublimation energies) with rigid molecular entities. The atomic force constant parameters were produced by fitting the available data for bond dissociation energies, spectroscopic data, and force constant data. Remaining atomic reference parameters for bonds and angles were then optimized by minimizing the force on all atoms in a range of over 600 experimental organic and organometallic crystal structures selected for their varied bonding chemistries.

We note that it is the nonbonding (i.e., electrostatic and van der Waals) terms which primarily determine the conformation of molecules; the role of the valence terms is to ensure that the fragments comprising the molecule have realistic geometries. How the fragments interact is described by the nonbonding terms. Furthermore, the conformations of the metallocene oligomers examined in this study are determined almost exclusively by the Coulomb energy as demonstrated later. Partial charges of the atoms have been included in Table 1. The remaining parameters are available as supporting information.

Description of Conformers in Terms of Torsion Angles. The conformations of bridged ferrocene oligomers may be concisely described by a number of torsion angles. Where the bridge consists of a single atom, as in the molecules discussed here, the relative disposition of any two neighboring ferrocenes is defined by two torsion angles; these are shown in Figure 3a and b. ϕ defines the rotation of the first ferrocene about the bond linking it to the bridging atom, whereas ψ describes the rotation of the second ferrocene about its bond to the bridge. Thus, all possible conformers of a bimetallic species are fully defined by ϕ and ψ. In the case of higher oligomers, however, there will be 1,1′-disubstituted ferrocene units; another dihedral, χ, shown in Figure 3c, is required to define the angle through which the substituents on the two rings are twisted away from one another. Thus, five torsion angles fully cover all the possible conformers of a trimetallic species. Taking the

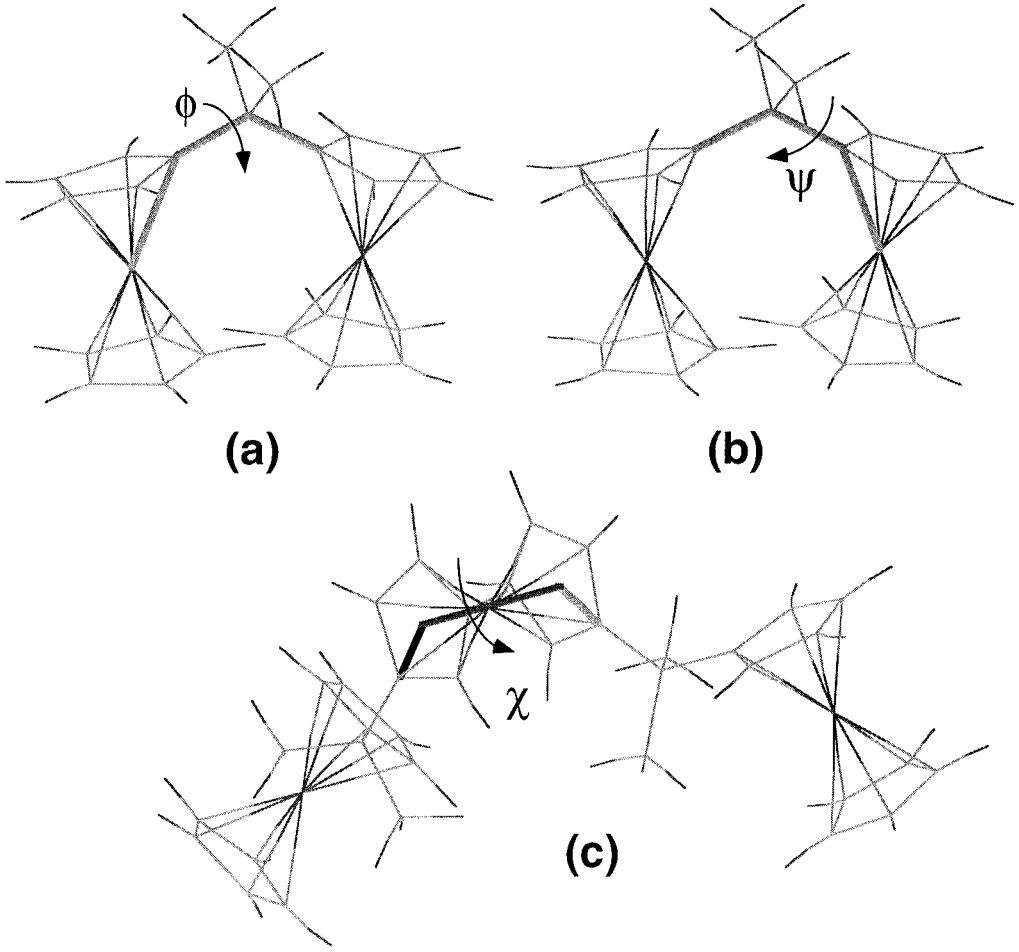

Figure 3. Definition of the torsion angles (a) ϕ, (b) ψ, and (c) χ.

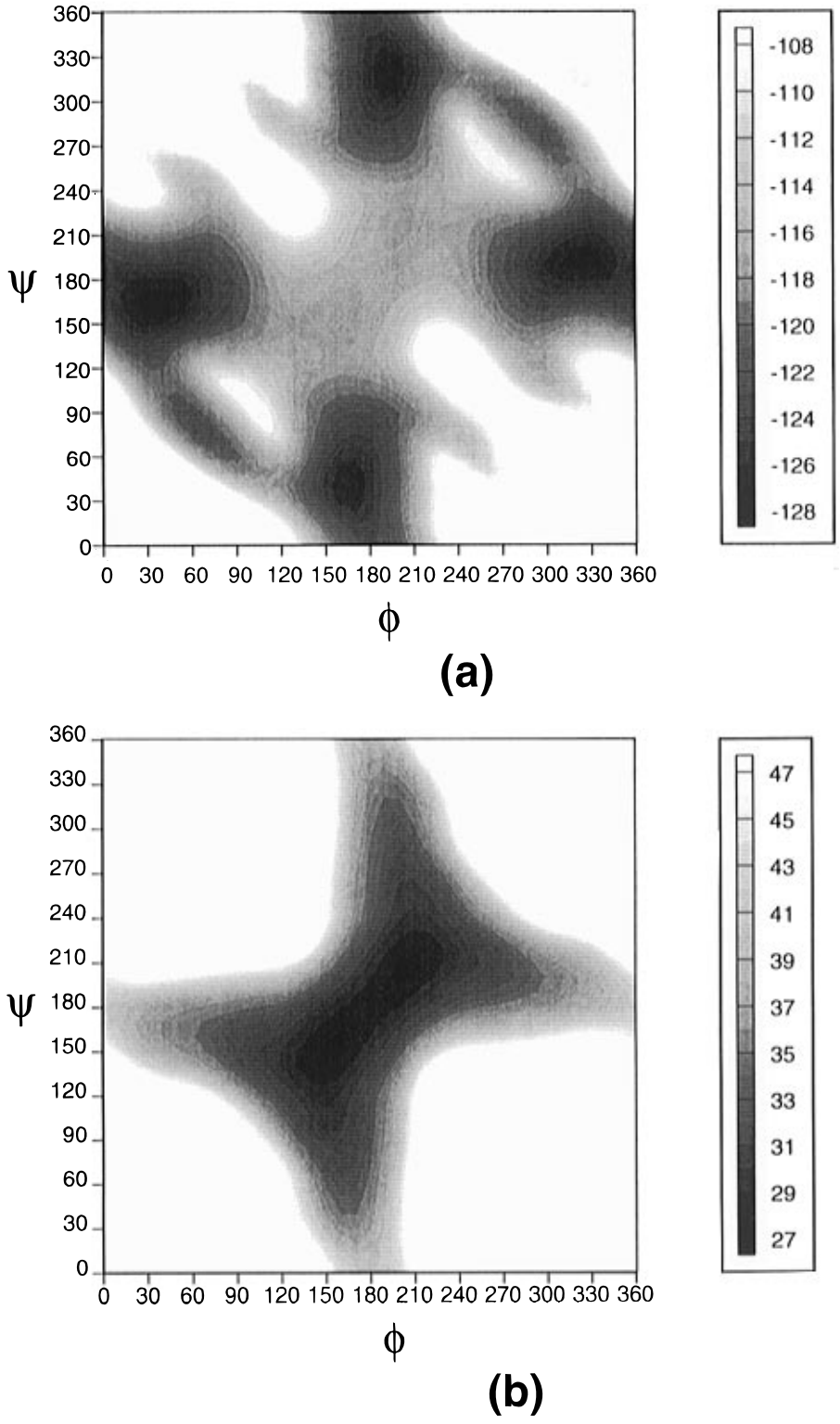

Figure 4. Plot of energy (kcal mol^{-1}) as a function of ϕ and ψ for (a) **1** and (b) $(\mathbf{1})^{2+}$.

molecule from one end, we have referred to these angles as ϕ_1, ψ_1, χ, ψ_2, and ϕ_2. For the pentamer, 11 angles are needed: three χ, four ϕ, and four ψ.

Calculation Strategies. Several strategies were employed in our investigation of the conformational preferences of ferrocene oligomers; all were performed using the Discover software.[43] In the simplest case, the energy was calculated for particular fixed conformations. The molecule was constructed in the desired conformation, and its energy was minimized with restraints employed to force the structure to retain the values of the relevant torsion angles throughout the minimization. Our second approach was to plot energy surfaces as a function of two torsion angles; this was achieved by systematic variation of the two angles in 10° increments from 0 to 360°. For each conformation the torsion angles were set to the required values and minimization carried out with these angles restrained. Any other torsion angles were restrained to a constant value for all of the conformations. For example, our plots of energy for centrosymmetric trimetallocenes involved 1369 combinations of ϕ and ψ. For each combination, Φ/Ψ, the molecule was adjusted to the required geometry and restraints imposed to force $\phi_1 = \Phi$, $\psi_1 = \Psi$, $\chi = 180°$, $\psi_2 = -\Psi$, and $\phi_2 = -\Phi$.

(43) *Discover 3.2*; developed and distributed by Molecular Simulations, Inc., 9685 Scranton Road, San Diego, CA 92121.

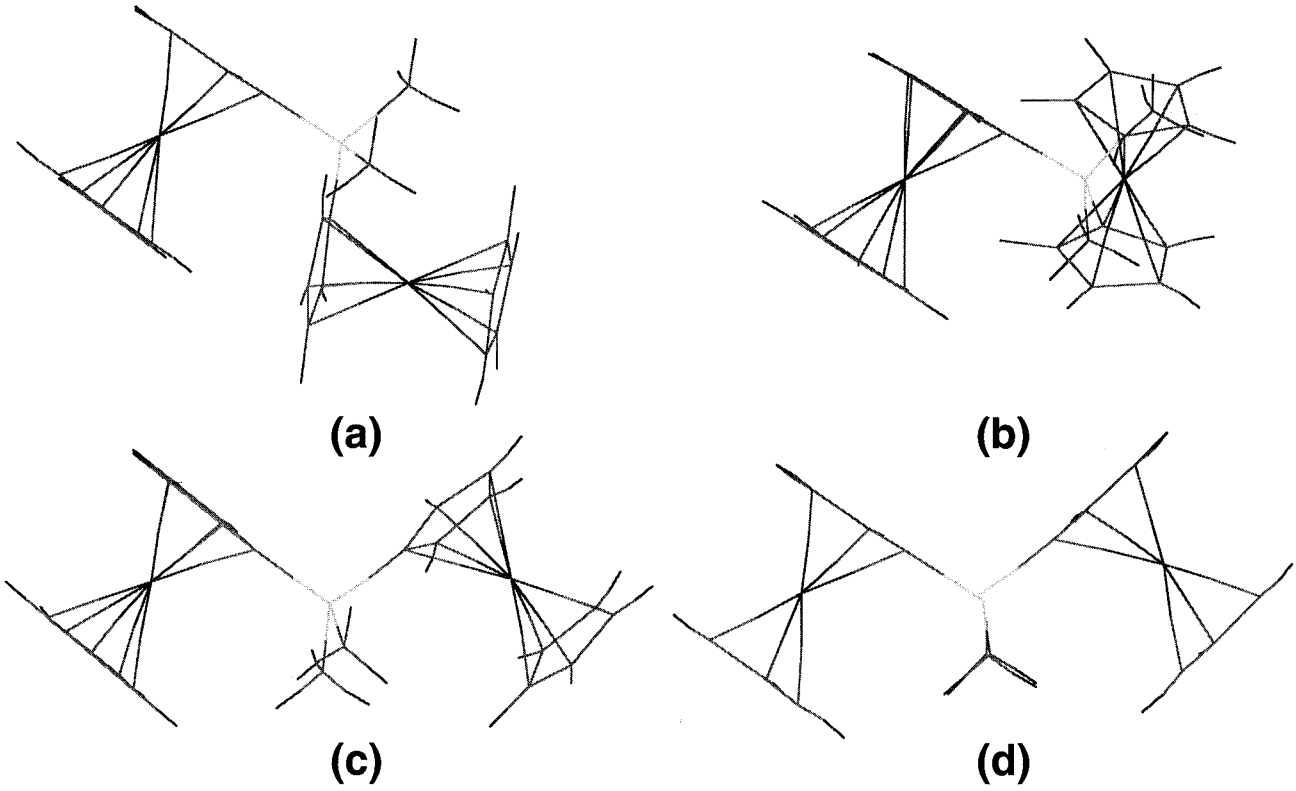

Figure 5. Conformers of **1**: (a)−(c) show the global, second and third minima respectively; (d) shows the conformation with $\phi = \psi = 180°$.

Table 2. Torsion Angles in the Experimental Structures of Trimetallics

structure	ϕ_1 (deg)	ψ_1 (deg)	χ (deg)	ψ_2 (deg)	ϕ_2 (deg)
3[23,24]	74	179	180	−179	−74
4[25]	168	56	89	177	−171
(**4**)$^{3+}$ [25]	175	174	174	174	175

Global minima were found by sampling a wide range of conformational space by molecular dynamics. The molecule was "heated" to 900 K for 5000 ps to produce an essentially random conformation. The energy of the molecule was then minimized from this random starting point with no restraints. The procedure was repeated 100 times for bi- and trimetallic species and 300 times for the pentamer.

Results and Discussion

Crystal Structure Torsion Angles. The relevant experimental structures are those of **3**,[23,24] **4**, (**4**)$^{3+}(CF_3SO_3^-)_3$,[25] and **5**.[14] The central iron atoms of both **3** and **5** lie on crystallographic inversion centers, whereas a molecule of **4** has a completely unsymmetrical conformation in the crystal structure and the central iron atom of the (**4**)$^{3+}$ cation lies on a crystallographic C_2 axis. As discussed above, the conformations of the oligometallocenes are defined by five torsion angles; these are summarized for the experimental trimetallic structures in Table 2. Eleven angles analogous to ϕ, ψ, and χ are are required to define the conformation of the pentamer **5**. The conformation in the crystal structure has $\phi_1 = -\phi_4 = -74°$, $\psi_1 = -\psi_4 = 174°$, $\chi_1 = -\chi_3 = 159°$, $\phi_2 = -\phi_3 = 167°$, $\psi_2 = -\psi_3 = 179°$, and $\chi_2 = 180°$.

Previous Modeling Study. The energies for three possible conformations of compound **3** were calculated in ref 24. These three conformers all possess inversion symmetry and, therefore, are characterized by $\phi_1 = -\phi_2$, $\psi_1 = -\psi_2$, and $\chi = 180°$. Table 3 shows the values of ϕ_1 and ψ_1 which define them together with the labels and calculated energies in the aforementioned work along with the energies from this study. These energies

Table 3. Comparison of Energies Calculated for Three Idealized Conformers (Relative to the Lowest Energy Conformer)

conformer	$\phi_1 = -\phi_2$ (deg)	$\psi_1 = -\psi_2$ (deg)	Pannell et al. (kcal mol^{-1})[24]	this work (kcal mol^{-1})
a	90	180	+126	0
b	90	90	+194	+2.1
c	180	180	0	+3.6

are expressed relative to the lowest energy conformer calculated in each case. As shown in Table 2, the conformation of **3** in the crystal structure most closely correspond to conformer **a**, which according to the previous calculations is less stable by more than 100 kcal mol^{-1} than conformer **c**. This energy difference is greater than the strength of a C−C single bond; it is therefore unrealistic and certainly could not be ascribed to crystal packing forces. However, we calculate that **a** has the lowest energy of these conformers and the difference in energy between the conformers is reasonable. Since it is not clear whether any of the three conformers corresponds to the global minimum of the isolated trimetallic or their cations, we performed extensive conformational analyses to examine this question.

Dimer. Before performing calculations on the trimetallic species, we looked at compound **1** (Figure 2), since its conformations are fully defined by only two torsion angles, ϕ and ψ. Thus the entire range of conformers can be depicted in a single plot of ϕ *vs* ψ and the global minimum assigned unambiguously. Figure 4 shows the resulting plots for both **1** and its dication. Both plots are highly symmetrical, possessing mirror planes along both diagonals. This high symmetry results from the indistinguishability of the two ferrocenes comprising the molecule, i.e., conformer ϕ/ψ is equivalent to ψ/ϕ. Furthermore, conformers ϕ/ψ and $-\phi/-\psi$ are mirror images of one another and thus have the same energy. As the size of the molecule is increased to three and then five ferrocenes, the symmetry is progressively lost as will be shown later. Figure 4 shows that the neutral dimer has two symmetry independent minima, whilst the dication has one. The global minima

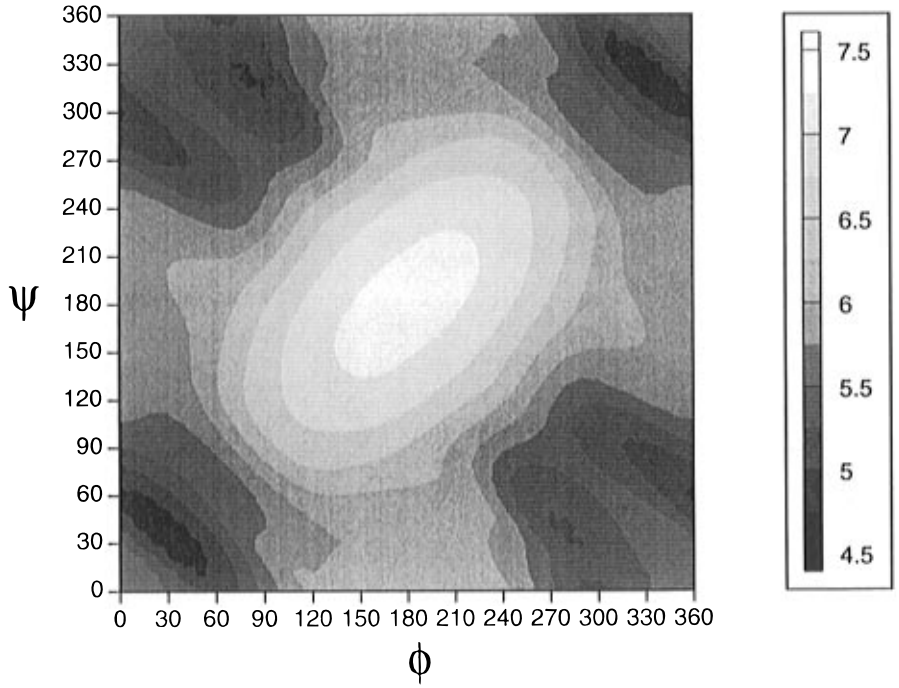

Figure 6. Plot of the Fe−Fe separation (Å) as a function of ϕ and ψ for **1**.

calculations find three minima for the neutral species; the lowest energy minimum at $\phi = 36°$, $\psi = 162°$ and the next minimum 1.0 kcal mol^{-1} higher at $\phi = \psi = 70°$. The third minimum, 3.9 kcal mol^{-1} higher than the global minimum, is found at $\phi = \psi = 167°$, though it is so shallow as not to be discernible in Figure 4. These minima were encountered 82, 14, and 4 times respectively, reflecting the width of the minima. For the dication, the only minimum occurs at $\phi = \psi = 163°$.

The three minima for the neutral molecule **1** are depicted in Figure 5 (parts a−c) together with the conformation corresponding to $\phi = \psi = 180°$ (Figure 5d). The principal axes of the two ferrocene units of the molecule in the lowest energy conformation are nearly perpendicular such that the substituted ring of one ferrocene unit closely approaches the iron center of the other. The second minimum can be considered as a distortion from the $\phi = \psi = 90°$ conformation. The third minimum is close to the idealized $\phi = \psi = 180°$ conformation, but with the two substituted rings twisted away from one another.

In an attempt to rationalize the positions of these minima, we examined them considering the iron atoms as centers of positive charge and the cyclopentadienyl rings as bearing negative charge. The dependence of the iron−iron separation on ϕ and ψ is drawn in Figure 6 and shows the maximum separation (7.09 Å) occurs at $\phi = \psi = 180°$. This is close to the conformation of the least stable of the three minima, which has an iron separation of 7.08 Å. The reason it distorts away from the $\phi = \psi = 180°$ geometry is to minimize the repulsion between the two negatively charged substituted rings. However, the global minimum corresponds to an intermediate iron−iron distance (5.95 Å), demonstrating that the iron−iron repulsion is not the overriding factor in determining the energies of the neutral dimer. In fact this conformation is determined by the attraction between the negatively charged substituted ring of one ferrocene and the positively charged iron atom of the other. The contribution of the electrostatic energy to the energy difference between the global and third minima is 3.0 kcal mol^{-1}, which accounts for 77% of the total energy difference. The closest approach of the substituted ring of one ferrocene and the iron of the other occurs at $\phi = 0°$, $\psi = 180°$; however, this conformation is destabilized by steric interference between the hydrogen atoms of the substituted ring with those of the unsubstituted ring of the other ferrocene. The second minimum is shallow and lies along the lowest energy pathway between the degenerate global minima $\phi = 36°$, $\psi = 162°$ and $\phi = 162°$, $\psi = 36°$; it has the rather short iron−iron separation of 5.61 Å. The principal contribution to the energy difference from the global minimum is again electrostatic (1.1 kcal mol^{-1}).

In contrast, the cation energies are determined primarily by the iron−iron repulsion, and hence the global minimum of (**1**)$^{2+}$, where the irons are separated by 7.19 Å, is close to the conformation with the maximum iron−iron distance (7.20 Å) at $\phi = \psi = 180°$. The distortion away from this idealized conformation is governed by repulsion between the substituted rings, as was the case for the third minimum of the neutral dimer.

For the carbon bridged analogue of **1**, denoted **2**, a plot of the energy surface is very similar to that for **1**. The global minimum of the neutral molecule was found at $\phi = 35°$, $\psi = 166°$. Subsidiary minima were found 2.4 kcal mol^{-1} above the global minimum at $\phi = \psi = 70°$ with an iron−iron separation of 5.33 Å, and 5.2 kcal mol^{-1} above the global minimum at $\phi = \psi = 162°$. In this case the third minimum is readily apparent in a plot of ϕ *vs* ψ. The three minima were encountered 82, 14, and 4 times, respectively. The (**2**)$^{2+}$ cation has a single minimum at $\phi = \psi = 155°$. In both the neutral and cationic cases, the minima of the carbon bridged species occur at very similar values of ϕ and ψ to those for the silicon bridged analogues. However, the energy surfaces are appreciably softer in the silicon cases, reflecting that the longer bridging bonds in the silicon compounds lead to greater separation between the ferrocene units.

Trimer. The conformations of the trimetallocenes can also be defined by two torsion angles, provided the central metal ion lies on an inversion center. Since the crystal structure of molecule **3** and the calculations of Pannell *et al.* satisfy this requirement, our initial studies focused on the centrosymmetric conformers. Figure 7 presents the energy surfaces for **3** and its trication. Both plots have C_2 symmetry reflecting the equivalence of ϕ/ψ with $-\phi/-\psi$, which are mirror images of one another. However, ϕ/ψ is no longer equivalent to ψ/ϕ since ϕ is the torsion angle about the bond from the terminal ferrocene

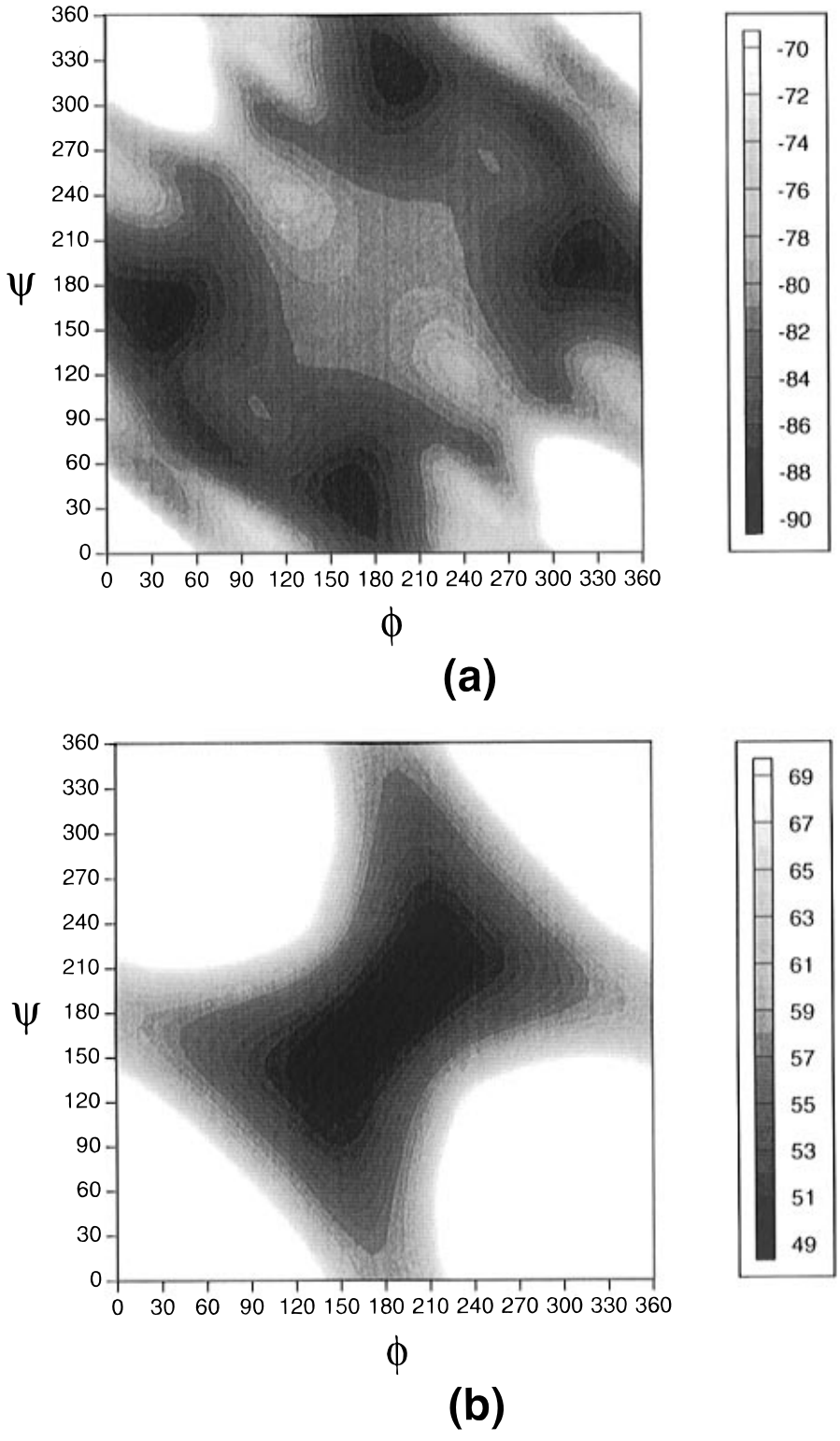

Figure 7. Plot of energy (kcal mol^{-1}) as a function of ϕ and ψ for centrosymmetric conformations of (a) **3** and (b) (**3**)$^{3+}$.

to the bridging atom, whereas ψ is the torsion angle about the bond from the central ferrocene to the bridge; clearly these are different. Despite this, both plots show approximately the same symmetry as those for the dimer. This reflects that, from an energetic viewpoint, the terminal and central ferrocenes are very similar.

The energy surface for centrosymmetric **3** closely resembles that for **1** (Figure 4), with minima at similar values of ϕ and ψ. The loss of symmetry described above produces two distinct deep minima of comparable but not identical energy. Interpolating, we find the minima at $\phi \approx 35°$, $\psi \approx 160°$ and $\phi \approx 165°$, $\psi \approx 30°$ with energies of approximately -88.3 and -88.0 kcal mol^{-1}, respectively. These minimum energy conformers are shown in Figure 8 (parts a and b). As was the case for the global minimum of the dimer, these minima allow close approach between negative cyclopentadienyl rings and positive iron centers. In particular, in the lowest energy minimum, the iron atoms of the terminal ferrocene units are near the rings of the central ferrocene. The other minimum corresponds to the opposite case where the iron of the central ferrocene is approached by the substituted rings of both terminal ferrocene units. Note that the latter case has a closer Cp$-$Cp distance between the substituted groups of the terminal ferrocenes which makes it slightly less stable than the former. As was the case

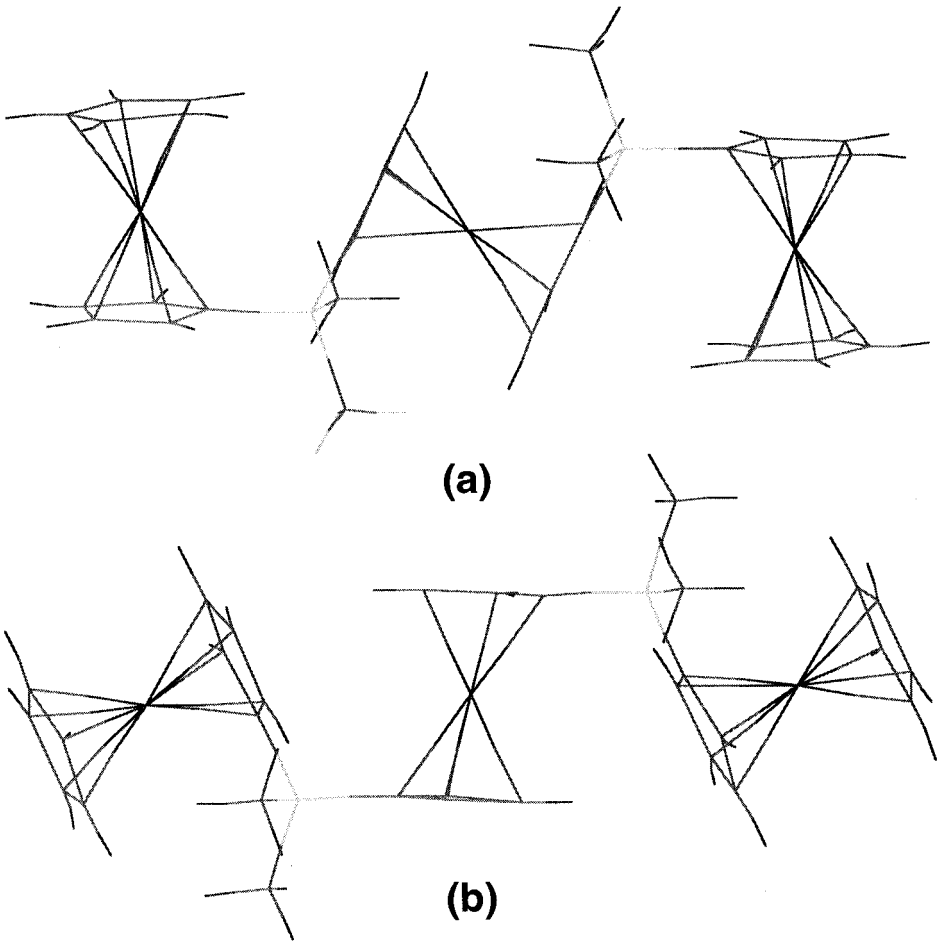

Figure 8. (a) The lowest and (b) second lowest energy centrosymmetric conformations of **3**.

Table 4. Energies and Torsion Angles for the Ten Lowest Energy Conformers of **3** Found in a Global Minimum Search

energy (kcal mol^{-1})	ϕ_1 (deg)	ψ_1 (deg)	χ (deg)	ψ_2 (deg)	ϕ_2 (deg)	freq (%)
−91.2	168	45	−116	75	67	2
−91.1	152	16	89	−77	−66	9
−90.7	161	35	−107	140	24	2
−90.7	163	36	−105	−179	−51	11
−90.4	159	13	79	176	48	9
−90.4	161	34	−118	34	161	2
−89.9	159	44	−97	−9	−171	5
−89.4	36	164	92	164	36	3
−89.3	34	130	−100	69	68	3
−89.1	36	164	90	−169	−35	3

for **1**, there is a low energy pathway connecting the two minima passing through $\phi \approx \psi \approx 70°$ although it is not clear if a minimum lies at this point.

It is not evident whether the minimum energy configuration will be centrosymmetric so we probed this issue by performing a global energy minimum search. These calculations revealed many minima, very close to one another in energy. The energies and angles for the ten lowest energy conformers are summarized in Table 4. Significantly none of these is centrosymmetric with χ significantly distorted from 180° in all cases, although two have C_2 symmetry. Most of the ϕ/ψ or ψ/ϕ combinations are distributed about either 35°/160° or 70°/70°, i.e., at similar positions to the lowest two minima for the dimer. Thus both the terminal ferrocene units interact favorably with the central ferrocene unit. The deviation of χ brings the two terminal ferrocenes into closer proximity thus allowing favorable electrostatic interactions between them, as can be seen in Figure 9a which shows the global minimum for **3**. In particular, the distance between the centroid of the substituted ring of one terminal ferrocene and the iron atom of the other is only 4.73 Å, which is comparable to the distance between the same centroid and the central iron atom of 4.59 Å. This contrasts with the case where both ϕ/ψ pairs are distributed around 35°/160° such as in the third minimum. Here the two close Cp centroid−Fe distances occur between the central ferrocene unit and the two end ferrocene units (4.34 Å and 4.39 Å) resulting in a much larger Cp−Fe distance between the two terminal groups (5.83 Å).

For the trication of **3**, the ϕ/ψ plot of the centrosymmetric conformations, reproduced in Figure 7b, shows a single very broad low energy region lying from 130°/130° to 230°/230°. This corresponds to distances between iron atoms in neighboring ferrocenes ranging from 7.08 Å to 7.24 Å. As was the case for the dimer cation, the very close energies in this region can be attributed to the compromise between iron−iron and Cp−Cp repulsion. The latter decreases as the former increases. The global minimum calculations located only one minimum, which has C_2 symmetry with $\phi_1 = \phi_2 = 165°$, $\psi_1 = \psi_2 = 163°$, and $\chi = 170°$. The ϕ and ψ angles are very close to those found for the $(\mathbf{1})^{2+}$ cation.

The energy plots for the centrosymmetric carbon-bridged species are shown in Figure 10. The plot for the neutral species is very similar to that for the silicon-bridged analogue, but the harder potential energy surface results in more minima being clearly resolved. The two deepest minima occur at similar ϕ/ψ angles to **3**, but are 0.5 kcal mol^{-1} different in energy. In contrast to Figure 7, the energy surface also displays two other distinct minima at positions analogous to those for **2**. These minima are at $\phi \approx 65°$, $\psi \approx 80°$ and $\phi \approx 160°$, $\psi \approx 150°$ and their respective energies lie approximately 5.4 and 10.0 kcal mol^{-1} above that of the deepest minimum. Global minimum

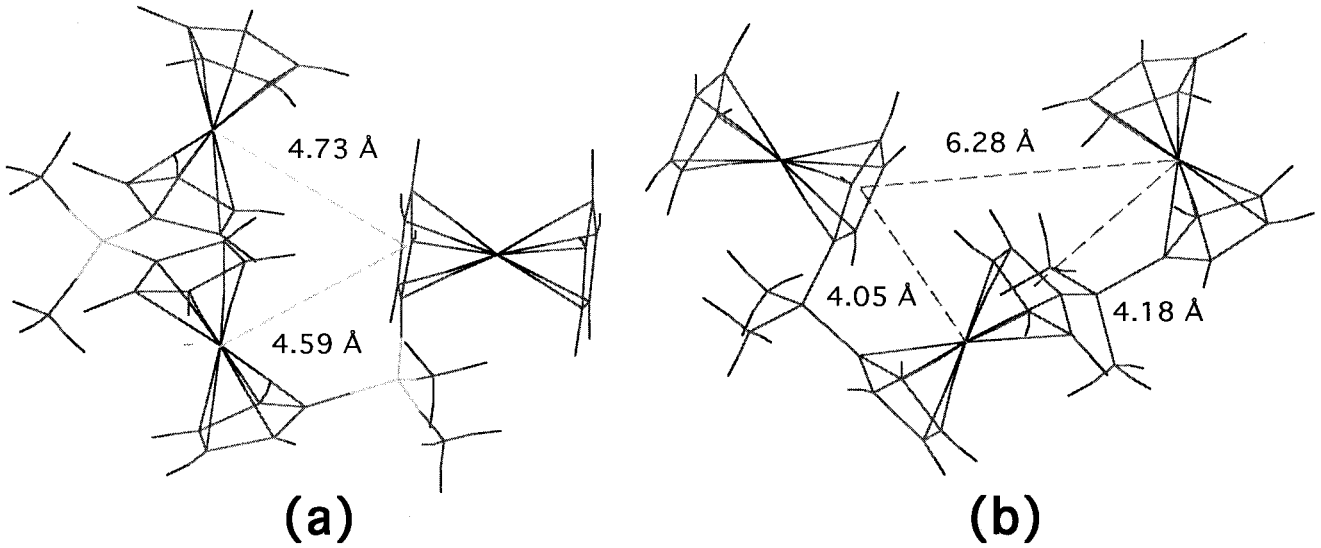

Figure 9. The global minima for (a) **3** and (b) **4** showing the close Cp−Fe distances between ferrocene units.

Table 5. Energies and Torsion Angles for the Ten Lowest Energy Conformers of **4** Found in a Global Minimum Search

energy (kcal mol^{-1})	ϕ_1 (deg)	ψ_1 (deg)	χ (deg)	ψ_2 (deg)	ϕ_2 (deg)	freq (%)
−128.8	165	34	−106	−176	−49	11
−128.6	165	33	−118	33	165	2
−128.6	164	33	−114	161	30	10
−128.4	163	26	89	170	40	6
−128.0	164	29	87	−168	−33	9
−127.9	169	31	99	−44	−166	10
−127.7	169	44	−118	72	69	2
−127.7	168	42	−120	64	78	2
−127.7	35	166	94	166	35	1
−127.5	165	36	92	36	165	2

calculations again revealed many minima, very close to one another in energy. The energies and angles for the ten lowest energy conformers are summarized in Table 5.

The global minimum for **4** has both sets of ϕ/ψ angles near 35°/160° producing two short Fe−Cp centroid distances of 4.05 and 4.18 Å between the central ferrocene unit and the two terminal ferrocenes as shown in Figure 9b. The shortest Fe−Cp distance between terminal groups is 6.28 Å. Examination of the seventh minimum shows that, in contrast to **3**, the combination of $\phi_1/\psi_1 \approx 35°/160°$ and $\phi_2 \approx \psi_2 \approx 70°$ does not permit terminal/terminal Fe−Cp distances comparable to the Fe−Cp distances possible between neighboring ferrocenes. This is a consequence of the shorter bridges in **4** arising from the shorter length of the C−C bond relative to the C−Si bond.

The energy plot for the centrosymmetric $(\mathbf{4})^{3+}$ cation is similar to that for $(\mathbf{3})^{3+}$, but two (symmetry equivalent) minima are resolvable in the low energy region at $\phi \approx \psi \approx 155°$ and $\phi \approx \psi \approx 205°$. Again, these angles represent decreasing the ring−ring repulsion at the expense of increasing iron−iron repulsion. Global minima calculations reveal three minima, the two lowest of which can, like the centrosymmetric minimum, be viewed as minor distortions from the ideal structure with all torsion angles at 180°. The global minimum, with energy 28.6 kcal mol^{-1}, was encountered 48 times; it has C_2 symmetry and is characterized by $\phi_1 = \phi_2 = 157°$, $\psi_1 = \psi_2 = 156°$, and $\chi = 173°$. The second minimum, with energy 28.7 kcal mol^{-1}, was encountered 35 times and is centrosymmetric with $\phi = 155°$, $\psi = 153°$. The third lies at 30.1 kcal mol^{-1} and was found 17 times; it has C_2 symmetry with $\phi_1 = \phi_2 = 152°$, $\psi_1 = \psi_2 = 142°$ and $\chi = 119°$. The three minima have distances between the iron atoms of neighboring ferrocenes of 6.73, 6.73, and 6.71 Å respectively, and between those of terminal ferrocenes of 13.46, 13.46, and 13.11 Å respectively.

Pentamer. For the pentametallic species, **5**, an 11-dimensional plot is needed to show all the possible conformations; even to show only the centrosymmetric conformers requires five dimensions. We therefore decided to begin our investigation of the conformational preferences of this molecule by probing distortions from the conformation found in the crystal structure. We were particularly interested to see if the interaction between two neighboring disubstituted ferrocenes was significantly different to that between a terminal ferrocene with another or with a bridging ferrocene (which we investigated in the dimer and trimer respectively). Figure 11 shows the energy plot for a centrosymmetric pentamer in which the configuration of the end pairs of ferrocenes are restrained to that found in the crystal ($\phi_1 = -\phi_4 = -74°$, $\psi_1 = -\psi_4 = 174°$, $\chi_1 = -\chi_3 = 159°$). The angles varied, $\phi_2 = -\phi_3$ and $\psi_2 = -\psi_3$, determine the relative disposition of the central ferrocene and its neighbors. The plot has no symmetry; now the conformation ϕ/ψ is inequivalent to $-\phi/-\psi$; they differ in the direction the end group is twisted relative to the central ferrocenes. However, the plot is broadly similar to that observed for **1** and **3**, with minima (now all inequivalent) at $\phi/\psi \approx 30/160°$, 165°/35°, 190°/330°, 320°/210°. Thus, the preferred relative dispositon of two nonterminal "chain" ferrocenes is very similar to the preferred terminal/neighbor orientation, again reflecting the importance of Fe−Cp electrostatic attractions.

The global minima search for **5** revealed a vast number of minima, the lowest of which is shown in Figure 12 and is over 15 kcal mol^{-1} more stable than the minimum in Figure 11. Again, the common feature of these minima is pairs of ϕ/ψ angles distributed around 35°/160° and, to a lesser extent, around 70°/70°, resulting in conformations with close Cp centroid−Fe distances within the oligomer chain and between the two terminal ferrocene groups. In the lowest energy case that we found $\phi_1 = 29°$, $\psi_1 = 143°$, $\chi_1 = -107°$, $\phi_2 = 32°$, $\psi_2 = 146$, $\chi_2 = 109°$, $\psi_3 = 48°$, $\phi_3 = 177°$, $\chi_3 = 99°$, $\psi_4 = -53°$, $\phi_4 = -167°$.

Summary and Discussion

We have studied the conformational preferences of isolated molecules of both neutral and oxidized oligo(ferrocenylsilanes). The energy range between extreme conformers is found to be much smaller than that calculated in ref 24. The conformations of the neutral species are principally determined by the

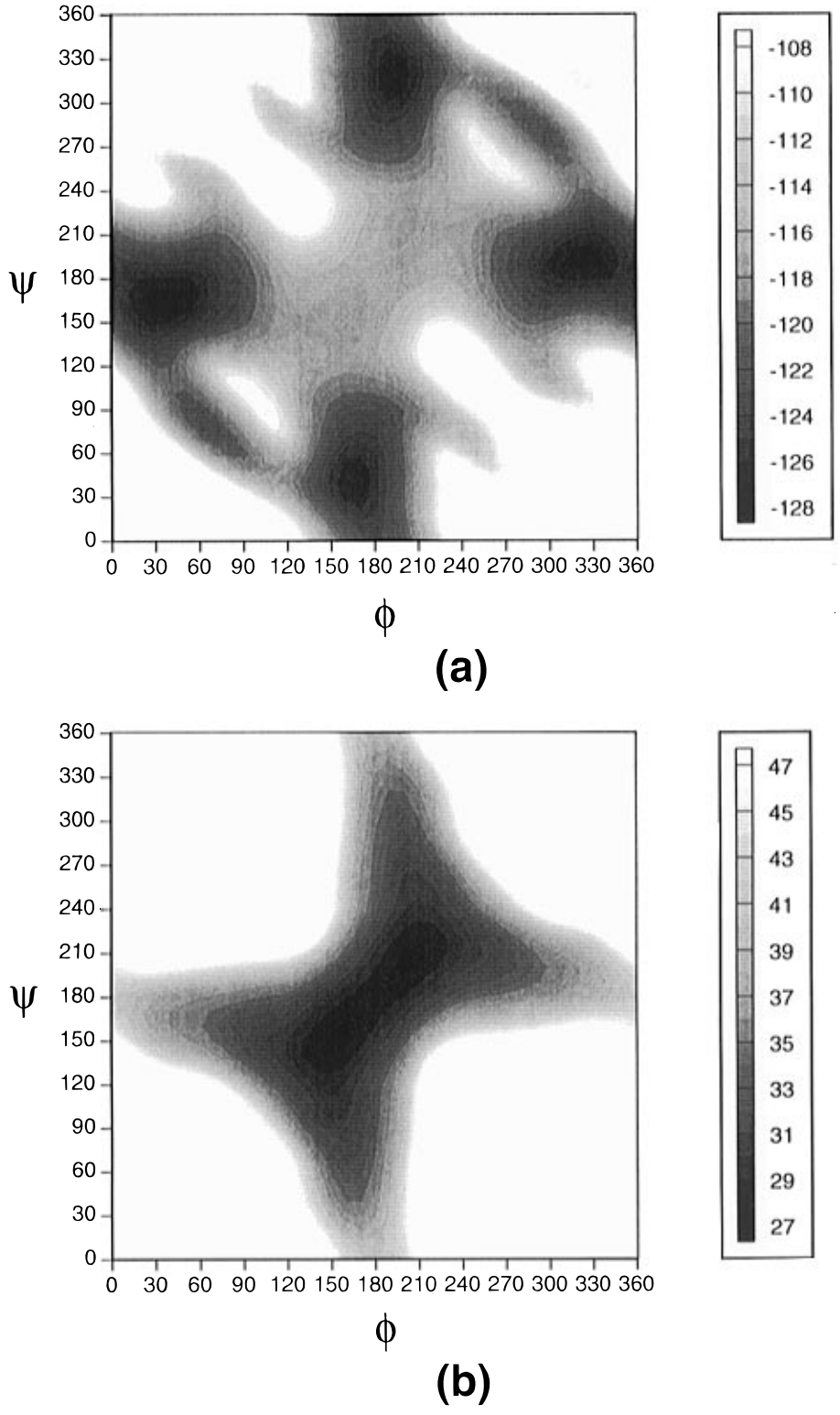

Figure 10. Plot of energy (kcal mol^{-1}) as a function of ϕ and ψ for centrosymmetric conformations of (a) **4** and (b) (**4**)$^{3+}$.

electrostatic attraction between the positively charged iron atoms of the ferrocene units and the negatively charged cyclopentadienyl rings of their neighbors. The lowest energy conformations for the trimetallic and pentametallic systems have strong Fe−Cp interactions between the ends of the molecule as well as between neighboring ferrocenes. In contrast, the conformations of the cationic derivatives of these species are principally determined by iron−iron repulsion, with some contribution from minimizing Cp−Cp repulsion.

We have also investigated the conformation preferences for the $SiEt_2$ bridged analogue of **3** and its trication; the energy surfaces are extremely similar to those for **3** with minima at almost identical angles and iron−iron distances. This suggests that differences in solution electrochemical behavior observed between $SiMe_2$ and $SiEt_2$ bridged polymers are electronic in nature, rather than due to differences in the preferred conformations of these species.

For the CMe_2 bridged analogues of the oligo(ferrocenylsilanes) broadly similar energy surfaces are found for both neutral and cationic species. However, the energy surfaces are appreciably harder in the carbon bridged species; this is principally because the C−C bond is shorter than the C−Si bond and so, for a given conformation, the ferrocene units are forced into closer proximity in the CMe_2 case than the $SiMe_2$ case.

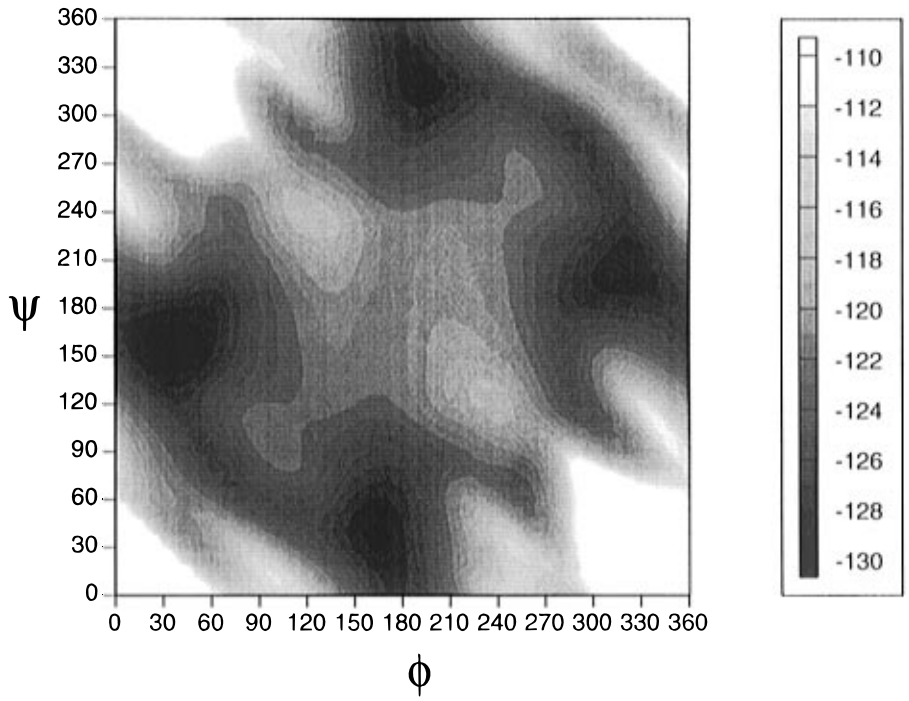

Figure 11. Plot of energy (kcal mol^{-1}) for centrosymmetric distortions of **5** fixing $\phi_1 = -\phi_4 = -74°$, $\psi_1 = -\psi_4 = 174°$, $\chi_1 = -\chi_3 = 159°$.

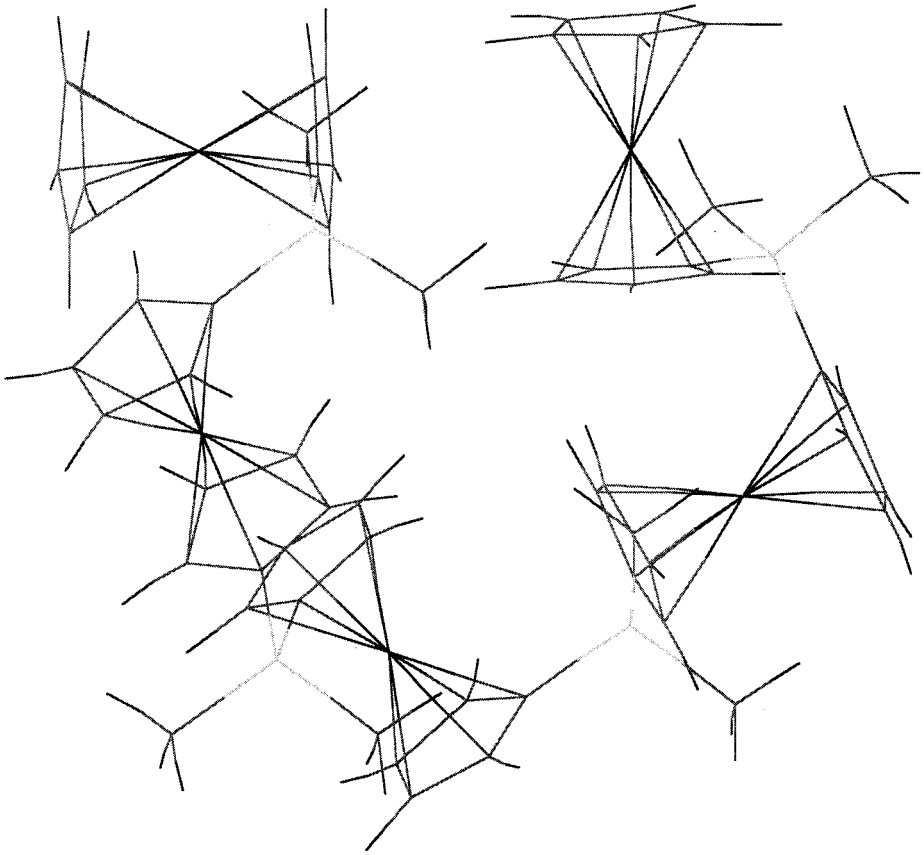

Figure 12. The lowest energy conformation for the pentamer **5**.

Crystal Structures. In the preceding section we have discussed the factors affecting the conformations of isolated molecules of oligometallocenes and their cations. However, the conformations observed in the experimental crystal structures do not correspond to the global minima we have found. We have therefore examined the crystal structures in more detail.

Crystal Structure of 3. An isolated molecule of **3**, with the torsion angles restrained to the values found in the crystal structure, has an energy of −85.1 kcal mol^{-1}. Although this is a lower energy than those we find for any of the idealized conformers in Table 3, it is significantly higher than that of the lowest minimum for centrosymmetric **3** (−88.3 kcal mol^{-1}) and the global minimum (−91.2 kcal mol^{-1}). Although the ϕ/ψ combination of 74°/179° allows some favorable interactions between the central iron atom and the substituted rings of the terminal ferrocenes, shorter Fe−Cp distances are found in the lowest centrosymmetric and global minima. However, in the crystal structure *inter*molecular interactions compensate for the loss of favorable *intra*molecular interactions. The packing consists of layers of molecules, within which the molecules are

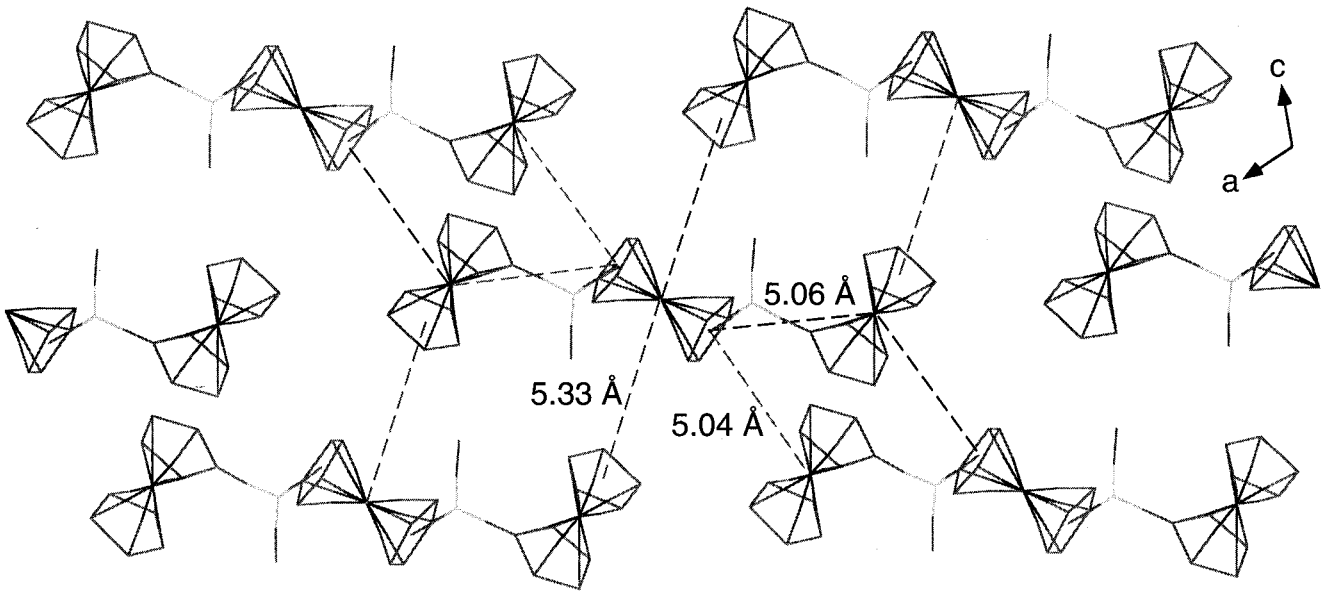

Figure 13. A layer of molecules in the crystal structure of **3** showing close Cp−Fe approaches around one of the molecules.

tilted relative to the plane of the layer. The molecules in adjacent layers are tilted in opposite directions, resulting in a herring bone stacking pattern perpendicular to the layers. A view of one layer is shown in Figure 13, together with the short Fe−Cp separations involving the central molecule. Clearly, this molecular conformation in this packing motif allows both intra- and intermolecular electrostatic Fe−Cp interactions. Since none of the ferrocene units has its axis oriented perpendicular to the plane of the layer, Fe−Cp interactions between adjacent layers are not possible. In fact, the relative disposition of two adjacent planes is principally determined by close-packing considerations.

Crystal Structure of 4. As in the case of **3**, an isolated molecule in the conformation found in the crystal structure (−121.6 kcal mol^{-1}) is somewhat higher in energy than the global minimum (−128.8 kcal mol^{-1}). Again, the crystal structure can be considered as the packing of layers, although they are more complex than that of **3** with each layer containing molecules in four different relative orientations. A view of a layer is shown in Figure 14, together with the close Fe−Cp contacts around one of the molecules. Again, the orientation of the axes of the ferrocene units does not permit electrostatic interactions *between* layers comparable to those *within* layers.

Crystal Structure of (4)$^{3+}$(CF$_3$SO$_3^-$)$_3$. An isolated (**4**)$^{3+}$ cation with the conformation found in the structure of the *tris*(triflate) has an energy of 29.2 kcal mol^{-1}, close to the 28.6 kcal mol^{-1} found for the global minimum. Like the global minimum, the conformation in the structure can be viewed as a distortion from the idealized $\phi_1 = \phi_2 = \psi_1 = \psi_2 = \chi = 180°$ conformation, with similar Fe−Fe separations (6.76 Å between the iron atoms of neighboring ferrocenes and 13.51 Å between those of the two terminal ferrocenes for the minimized cation with torsion angles restrained to those in the crystal structure compared to 6.73 and 13.46 Å, respectively, in the global minimum). The conformations of the cations are principally determined by Fe−Fe repulsion; *intra*cation forces will also be repulsive. In this case, it appears that packing considerations have very minor effects on the "isolated" conformation. A very similar conformation is found for the cation in the structure of [(Fc″CH$_2$C$_5$H$_4$)$_2$Co]$^{3+}$[TCNE$^-$]$_3$ (Fc″ = octamethylferrocenyl; TCNE = tetracyanoethylene).[25]

Crystal Structure of 5. As in the case of **3** and **4**, the structure of **5** can be viewed in terms of layers; although in this case the molecules lie almost parallel to the plane of the layers. A layer of **5** is illustrated in Figure 15 and shows that even closer intermolecular Fe−Cp approaches than those in the structure of **3** are found. In this case, the twist of each terminal group allows close approach of its iron atom to the rings of two chain ferrocenes in an adjacent molecule. Since **5** has an odd number of ferrocene moieties, the terminal groups are oriented in opposite directions, allowing each molecule to have close Fe−Cp approaches to two neighbors. Such good intermolecular interactions would not be possible for an even number of ferrocenes as the terminal ferrocenes would have the same orientation and therefore only be able to have close Fe−Cp contacts with one neighbor. Interestingly, although the tetramer, hexamer, and octamer have been isolated,[14] no crystal structures have been yet reported. Furthermore, in **3** it is not possible for the terminal groups to adopt this arrangement as each molecule has only one chain ferrocene; thus the terminal ferrocenes twist to allow favorable interactions with several neighboring ferrocenes. If the layers in Figures 13 and 15 are both viewed as molecules lying side to side to form ribbons running bottom left to top right, then **3** has both intra- and interribbon Fe−Cp interactions, whereas **5** has only intraribbon interactions. In addition, the "flatter" layers, coupled with the twist of the end ferrocenes, allows some favorable interlayer Fe−Cp interactions. However, they cannot be ideally aligned as a molecule in the layer above must lie across the interribbon boundary which makes the spacings between its ferrocene units incommensurate with those of the two molecules in the layer below.

Calculations. Can energy calculations explain why the two neutral trimers **3** and **4** adopt different packing motifs? A good test of a potential parameter set is to see if it can reproduce the experimental crystal structures. The cell parameters for **3**, **4**, and **5** calculated using the ESFF forcefield are summarized in Table 6. These were obtained by full relaxation of the atomic coordinates and cell parameters of the experimental structures using the same potentials used for the isolated conformer calculations, with no restraints on the molecules and with no symmetry within the unit cell. Convergence acceleration (the Ewald method) was used for both Coulombic and van der Waals interaction terms.[44] For **3**, the root mean square deviation (rmsd) between the crystallographic and calculated bond lengths (of which there are 68 excluding bonds to hydrogen) is 0.08 Å. For the bond angles (of which there are 249) the rmsd is 5.8° which falls to 2.0° if the C−Fe−C angles are excluded (these angles are extremely sensitive to the relative rotation of the rings

(44) Williams, D. E. *Acta Crystallogr.* **1971**, *C51*, 452.

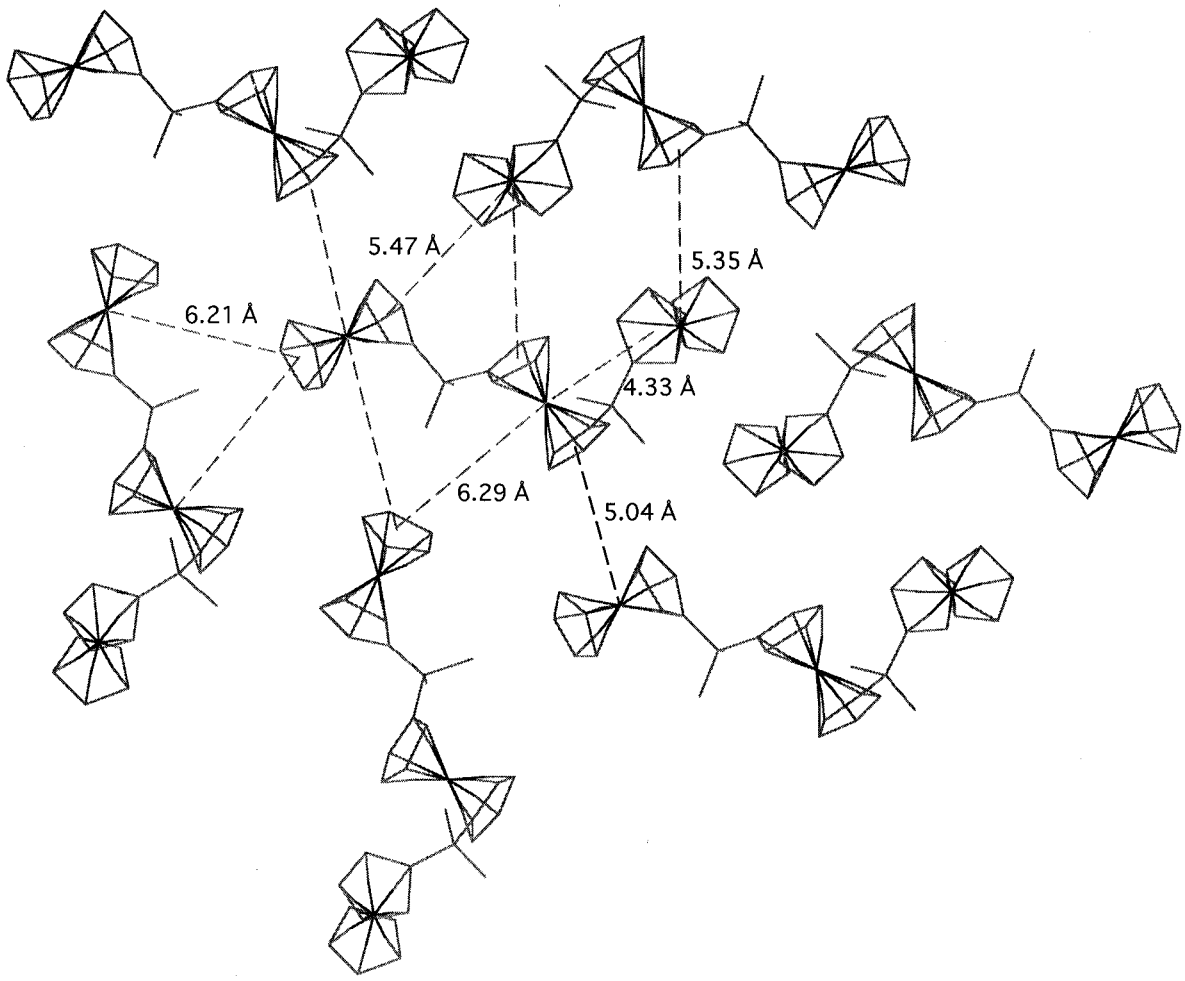

Figure 14. A layer of molecules in the crystal structure of **4** showing close Cp−Fe approaches around one of the molecules.

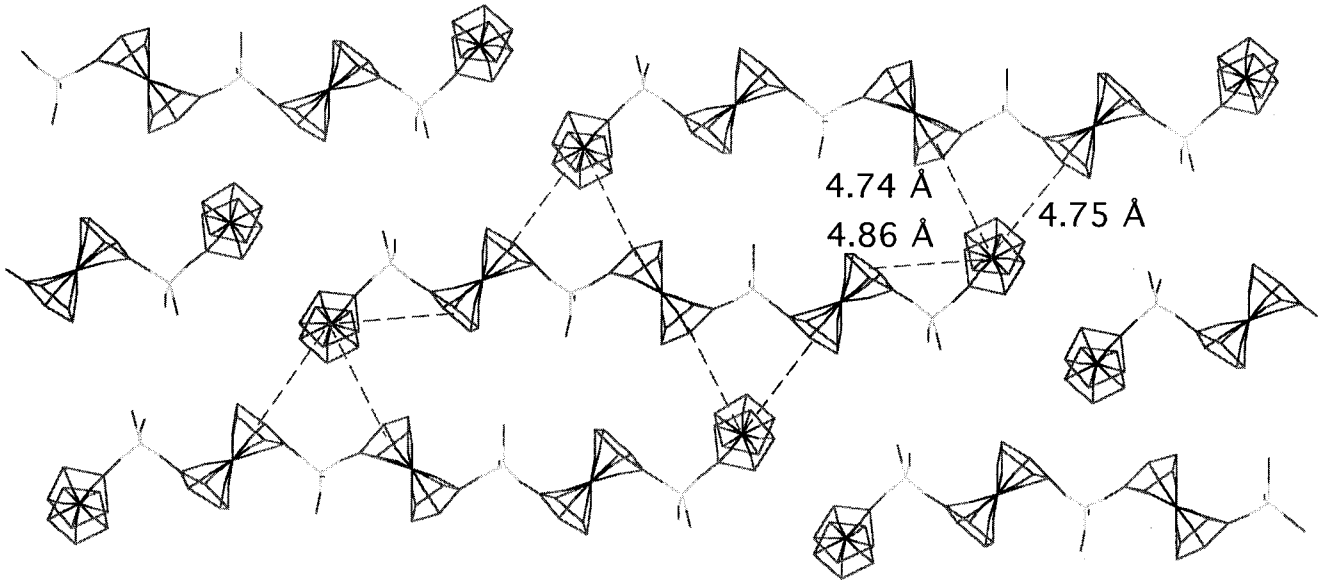

Figure 15. A layer of molecules in the crystal structure of **5** showing close Cp−Fe approaches around one of the molecules.

which are better described in terms of torsional angles). Similar results were obtained for the other structures. Reassuringly, the cells of both **3** and **4** stayed monoclinic although the change in cell dimensions is smaller for **3** (average of the absolute deviation of 1.9%) than **4** (3.9%). Note, however, that the molecular inversion center in **3** is lost. Both molecules of **3** in the unit cell have conformations defined by $\phi_1 = 82°$, $\psi_1 = 170°$, $\chi = 163°$, $\psi_2 = -184°$, and $\psi_2 = -62°$ (cf. experimental values in Table 2). For **4**, the torsion angles have changed to 168°, 53°, 88°, 184°, and −170°. For **5** the new angles are $\phi_1 = -\phi_4 = -78°$, $\psi_1 = -\psi_4 = 176°$, $\chi_1 = -\chi_3 = 177°$, $\phi_2 = -\phi_3 = 174°$, $\psi_2 = -\psi_3 = 172°$, and $\chi_2 = 180°$. Thus agreement between experiment and calculations is very good, especially considering that the potentials have not been fitted in any way to structures of this type.

To test if energy calculations can provide insight into the two packing motifs for the trimers, we placed molecule **4** into the packing arrangement of **3** and minimized the structure. The final energy was 6.2 kcal mol^{-1} lower in energy, i.e., the potentials predict that molecule **4** would rather adopt the crystal

Table 6. Calculated and Experimental Lattice constants of **3**, **4**, and **5**

	structure 3		structure 4		structure 5	
parameter	exptl	calcd	exptl	calcd	exptl	calcd
a (Å)	10.084	10.051	14.409	14.897	11.764	11.732
b (Å)	14.958	14.835	11.583	11.906	11.85	12.016
c (Å)	11.175	10.658	16.979	16.053	12.514	11.781
α (deg)	90	90.000	90	90.000	94.85	93.86
β (deg)	114.98	112.71	92.212	88.392	114.15	118.03
γ (deg)	90	90.000	90	90.000	117.66	114.23

structure of **3**. However, placing **3** in the structure of **4** and minimizing resulted in a higher energy structure. It is perhaps not too surprising that the potentials are unable to predict two different structures for two molecules which are so similar; only the highest quality potentials would be able to make this distinction.

Summary and Discussion

Examination of the experimental crystal structures for the neutral oligometallocenes **3**, **4** and **5** reveals different conformations to the lowest energy conformers for the isolated species. However, the solid state conformations allow *inter*molecular interactions between negatively charged cyclopentadienyl rings and iron atoms comparable to the *intra*molecular interactions found for the low energy conformers of the isolated species.

Powder X-ray diffraction studies of **5** show a dominant peak at a d-spacing, indexed as the (011) reflection, corresponding to diffraction from the layers of molecules depicted in Figure 15. The principal feature in the diffraction pattern of the polymer, $[Fe(C_5H_4)_2SiMe_2]_n$, is a broad peak centered around the same d-spacing.[6,15] This has been interpreted as evidence that the structures of the polymer and the pentamer are related.[15] Our calculations suggest that polymer molecules could adopt a similar layer structure to **5**, but we expect that some of the chain ferrocenes will be twisted approximately perpendicular to the layers in a similar fashion to the terminal ferrocenes of **5**. This would allow close iron−cyclopentadienyl interactions between adjacent polymer chains within a layer. The arrangement in the pentamer suggests that the polymer structure where every fifth ferrocene is twisted approximately perpendicular to the plane would allow a particularly good network of favorable Fe−Cp interactions. Similarly, we would expect the nonameric species to crystallize into a layer structure with the first, fifth and ninth ferrocenes twisted perpendicular to the plane of the layer.

The structure of the $(\mathbf{4})^{3+}$ cation shows the conformation of the cation to be very similar to that calculated for the isolated species. As the Fe−Fe repulsion is the dominant energy term in determining the conformation, packing forces have little effect in this structure.

Conclusions

The ESFF forcefield has been shown to be a useful method for understanding and predicting the conformations of oligomeric metallocene species; both as isolated molecules and in the solid state. The conformations of neutral species are principally determined by Fe−Cp electrostatic interactions. The possibility of intermolecular Fe−Cp attractions in the solid state leads to different conformations being found in crystal structures to those predicted for isolated molecules. The conformations of oxidized species are principally determined by repulsion between the centers of positive charge.

Acknowledgment. S.B. thanks the EPSRC for a studentship, and A.L.R. is most grateful to The Ramsay Trust and British Gas for his Ramsay Fellowship.

Supporting Information Available: Tables of bond energies, bond angles, torsion angles, and van der Waals parameters (2 pages). See any current masthead page for ordering and Internet access instructions.

JA953680S